Nonlinear pulse combining and pulse compression in multi-core fibers

A. M. Rubenchik,[1] I. S. Chekhovskoy,[2,3,*] M. P. Fedoruk,[2,3] O. V. Shtyrina,[2,3] and S. K. Turitsyn[2,4]

[1]Lawrence Livermore National Laboratory, Livermore, California 94550, USA

[2]Novosibirsk State University, Novosibirsk 630090, Russia

[3]Institute for Computational Technologies, SB RAS, Novosibirsk 630090, Russia

[4]Aston Institute of Photonic Technologies, Aston University, Birmingham B4 7ET, UK

*Corresponding author: igor428m@gmail.com

Received November 5, 2014; revised January 9, 2015; accepted January 10, 2015;
posted January 14, 2015 (Doc. ID 226315); published February 17, 2015

We demonstrate light pulse combining and pulse compression using a continuous-discrete nonlinear system implemented in a multi-core fiber (MCF). It is shown that the pulses initially injected into all of the cores of a ring MCF are combined by nonlinearity into a small number of cores with simultaneous pulse compression. We demonstrate the combining of 77% of the energy into one core with pulse compression over 14× in a 20-core MCF. We also demonstrate that a suggested scheme is insensitive to the phase perturbations. Nonlinear spatio-temporal pulse manipulation in multi-core fibers can be exploited for various applications, including pulse compression, switching, and combining.

OCIS codes: (190.4360) Nonlinear optics, devices; (060.4370) Nonlinear optics, fibers.
http://dx.doi.org/10.1364/OL.40.000721

Optical multi-core fibers (MCFs) have recently attracted a great deal of attention in the context of spatial-division multiplexing for high-capacity optical communications (see [1,2] and references therein). In conventional optical communications, the nonlinear effects that occur during signal propagation in a fiber are somewhat undesirable.

However, at a high signal power, developed MCFs can be also considered to be a nonlinear discrete physical system, which is interesting for both fundamental science [3,4] and for practical applications, such as nonlinear photonic devices [5–7]. In particular, the nonlinear-induced collapse (self-focusing, blow-up) of the initial wave packet can be used for pulse compression [8]. The theoretical background for such an approach in the case of nonlinear discrete optical arrays has been developed in [6,7]. It has been shown in [6,7] that wave collapse leads to the localization of energy in a small number of cores with simultaneous amplification and compression.

The nonlinear dynamics in MCFs has an interesting link with the light bullets (LBs) proposed in [9]. The LBs in waveguide arrays have been recently demonstrated and studied in [10,11]. The LBs studied in [10,11] are discrete optical spatio-temporal solitons. A discrete-continuous system, such as a MCF, may prevent the wave collapse that is typical for light dynamics in a multidimensional continuous nonlinear medium [12,13]. In this Letter, we demonstrate that nonlinear energy localization in MCFs may be used for pulse combining and compression. We consider the optical MCFs with the circular ring symmetry of their cores shown in Fig. 1. Note that many of the obtained results are generic, and are applicable to various other MCF configurations.

The propagation of light down a MCF can be approximately (neglecting polarization characteristics for the sake of clarity) described as a superposition of modes localized at each core:

$$E(x,y,z,t)=\sum_k A_k(z,t)F_k(x-x_k,y-y_k)e^{i(\beta_k z-\omega t)}+\text{cc}, \quad (1)$$

where F_k is the spatial mode structure and A_k is the envelope of the electromagnetic field in the kth core. In the limit of a weak coupling approximation, one can derive a system of equations for the envelopes A_k, i.e., the continuous-discrete nonlinear Schrödinger equation [14]:

$$i\frac{\partial A_k}{\partial z}=\frac{\beta_2^k}{2}\frac{\partial^2 A_k}{\partial t^2}-\gamma_k|A_k|^2A_k-\sum_{m=1}^{N}C_{km}A_m. \quad (2)$$

Here $k=1,\ldots,N$, β_2^k is the group-velocity dispersion parameter for the mode k, γ_k is the Kerr parameter, and C_{km} represents the coupling coefficients between the cores.

System (2) can be simplified for the identical cores, as discussed in [6,7]. Taking into account the most important physical effects, we can simplify the analysis with the following assumption:

$$C_{kk}=C_1>0, \qquad C_{k,k+1}=C>0 \quad (3)$$

while neglecting all other coupling terms. For the sake of clarity, we consider $\beta_2^k=\beta_2$, $\gamma_k=\gamma$ $(k=1,\ldots,N)$ in what

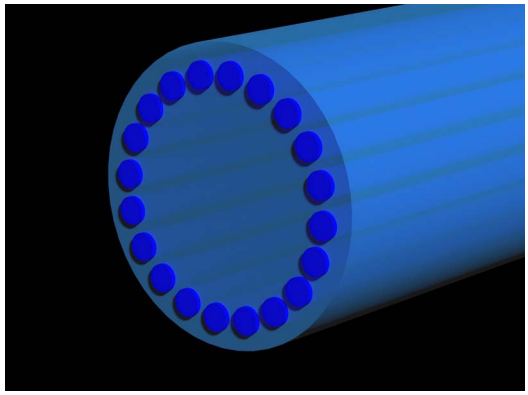

Fig. 1. Schematic depiction of the considered MCF waveguide with the cores arranged in a circle.

follows; however, the results can be easily extended to more general cases.

It is convenient to introduce normalized variables, such as $A_k = \sqrt{(C/\gamma)}U_k e^{i(2+C_1/C)z'}$, where $z' = z/L$, $L = 1/C$, $t' = t/T$, and $T^2 = -\beta_2/(2C)$. The dimensionless equations (omitting the primes) read:

$$i\frac{\partial U_k}{\partial z} = -\frac{\partial^2 U_k}{\partial t^2} - (U_{k+1} - 2U_k + U_{k-1}) - |U_k|^2 U_k. \quad (4)$$

The system (4) is the Hamiltonian equation

$$i\frac{\partial U_k}{\partial z} = \frac{\delta H}{\delta U_k^*} \quad (5)$$

with

$$H = \sum_{k=1}^{N}\int_{-\infty}^{\infty}\left[\left|\frac{\partial U_k}{\partial t}\right|^2 + |U_k - U_{k-1}|^2 - \frac{|U_k|^4}{2}\right]\mathrm{d}t. \quad (6)$$

The system (4) conserves H and total energy (normalized by C/γ)

$$E_t = \sum_{k=1}^{N}\int_{-\infty}^{\infty}|U_k(z,t)|^2\mathrm{d}t. \quad (7)$$

To understand qualitatively the evolution of the pulses injected into an MCF, consider first a system with a large N and smooth intensity distribution that experiences only small changes between neighboring cores. In this case, we can derive the continuous version of Eq. (4) for $U(k,t,z)$

$$i\frac{\partial U}{\partial z} + \frac{\partial^2 U}{\partial t^2} + \frac{\partial^2 U}{\partial k^2} + |U|^2 U = 0, \quad (8)$$

and

$$H = \int_{-\infty}^{\infty}\left[\left|\frac{\partial U}{\partial t}\right|^2 + \left|\frac{\partial U}{\partial k}\right|^2 - \frac{|U|^4}{2}\right]\mathrm{d}t. \quad (9)$$

Equation (8) is equivalent to the nonlinear Schrödinger equation (NLSE) that describes the self-focusing property of light in a nonlinear media. If the power at the entrance to the MCF exceeds the critical value $P_{\mathrm{cr}} = 4\pi$, making $H < 0$, the intensity distribution is self-compressed over k and t. We can expect that the injected MCF pulses distributed over the cores with smooth maxima will be focused into a few cores around the maxima with simultaneous pulse compression. When the energy is concentrated into a few cores, the discreteness of the cores arrests further compression.

This scenario has been verified via numerical experiments. In our modeling, we have used the same Gaussian pulses in each core, but slightly perturbed the amplitudes from core to core to initiate an instability:

$$U_k = \sqrt{P}\exp\left(\frac{-t^2}{2\tau^2}\right)\left[1 + 0.03\cos\left(\frac{2\pi k}{N}\right)\right]. \quad (10)$$

The corresponding distribution of the total energy E_t over the cores is symmetrical with respect to the Nth core. It has one maximum at $k = N$, with the symmetry between $k = l$ and $k = N - l$. As a result, we will plot the information for only half of the cores. In the numerical computations, we used the split-step Fourier method with the Pade approximation with scaling and squaring for the matrix exponent (see [15,16]).

To compress the input light distribution as a whole, the fastest-growing mode must be about the size of the system. From the analysis of plane wave instability, we estimate that the input is $U \sim \sqrt{P} \sim 2/N \sim 1/\tau$. We used this simple estimate to guide our choice of the initial pulse width and energy. A higher amplitude U results in the breakdown of the distribution into a few bunches.

As can be seen from the initial conditions [Eq. (10)], the pulse amplitudes are perturbed by no more than 3%. The increase of the initial modulation (as long as it is still small) does not effect the qualitative behavior, but it does accelerate the process development.

The evolution of the Gaussian pulses Eq. (10) for $N = 6$ is presented in Fig. 2. One can see the combining of almost all of the injected energy into one of the pulses with simultaneous pulse compression. For the specific case presented in Fig. 2, with the parameters $P = 0.61$ and $\tau = 1.5$, we observed that the peak power increased to 30.6×, with pulse duration compressions of 6.6×. The maximum compression is reached at $z = z_0 = 33.3$. One can see that at $z_0 = 33.3$, ~82.8% of the initial energy is concentrated into a single core. Further propagation leads to the periodic oscillating of the light intensity. This is the result of the conservation of the Hamiltonian H, which is, in general, different at the input from the value at a steady state. Therefore, part of the energy should go into oscillations. It is important to note that the energy continues to be localized in a few cores, forming nonstationary LBs. In terms of practical applications, the input

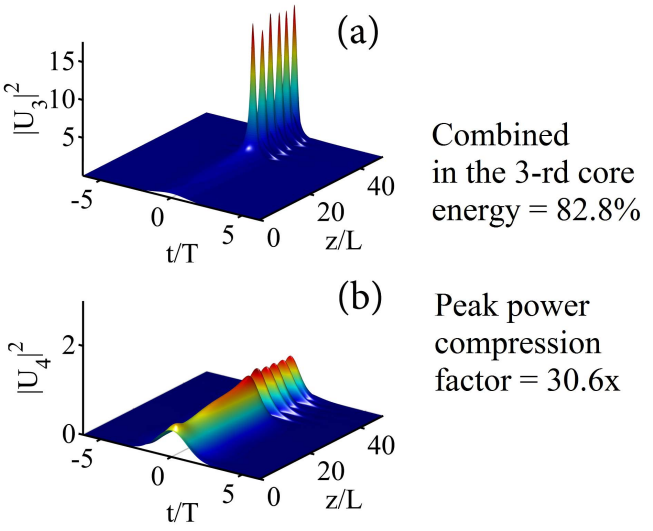

Fig. 2. Evolution of the input Gaussian pulses [Eq. (10)] with the parameters $P = 0.61$ and $\tau = 1.5$ is shown for the third core, where most of energy is concentrated after propagation. As an example of the dynamics in the neighboring cores of the 6-core fiber, the fourth core is also shown. Note the different power scales for the third and fourth cores.

power and the length of the MCF device should be carefully designed to achieve the maximum pulse compression and energy combining.

The evolution of the peak amplitudes and pulse durations in different cores is presented in Fig. 3. A very important point is that compression does not degrade the beam shape. The initial pulse profile and waveform after compression are presented in Fig. 4. One can see that small shape deformations are confined to the wings, and occur only when the intensity is less then 0.6% of the peak.

The increase of the initial modulation depth from 0.03 to 0.3 does not qualitatively change the evolution, peak intensity, or pulse compression. However, it does accelerate the process, and reduces z_0 to 3.9.

The calculation for $N = 20$, with optimal parameters of $P = 0.08035$ and $\tau = 3.85$ and a modulation of 0.03, results in similar behavior (see Fig. 3). In this case, the intensity is lower to suppress the development of small scale perturbations, and the peak compression takes place at the longer distance $z_0 = 115.2$. Increasing the number of cores reduces the pulse width and increases intensity. For a 20-core MCF, the pulse width compression factor is around 17.4×, while the peak power in the compressed pulse is increased by 206×. The percentage of the power combined in one core is 72.7%.

Figure 5 depicts the spatial density distribution of the total energy E_t over the cores at the distance of maximum compression for the 6-core and 20-core MCFs. For a large N, the evolution leading to compression happens at long distance. In general, we may expect losses to occur during the compression when the power is in excess of P_{cr}. One can see that at the peak of compression, the ratio of the peak intensity to the intensity in the neighboring cores is higher for $N = 6$ than for $N = 20$ (28.1× against 22.4×), as seen in Fig. 5.

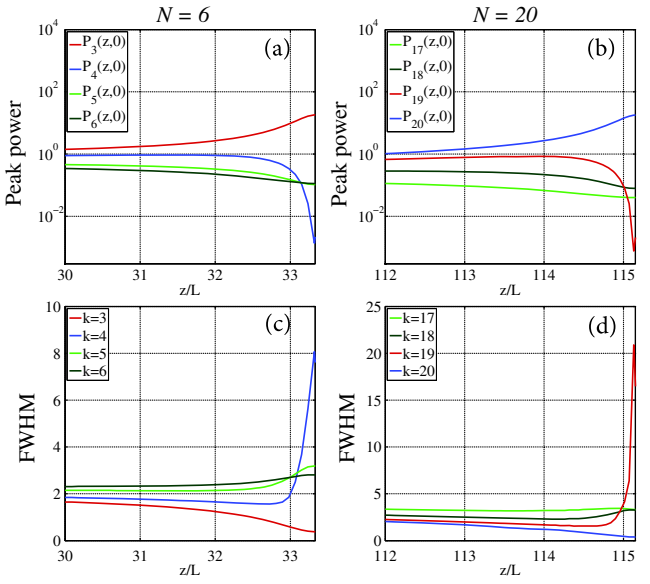

Fig. 3. (a) The dynamic of the peak powers (upper pictures) and pulse widths (bottom pictures) of the input Gaussian pulses [Eq. (10)] with parameters $P = 0.61$ and $\tau = 1.5$ in 3rd—6th cores of a 6-core MCF (a and c) and pulses with parameters $P = 0.08035$ and $\tau = 3.85$ in the 17th—20th cores for a 20-core MCF (b and d). Graphs (c) and (d) show the dynamics of full width at half maximum of the corresponding pulses.

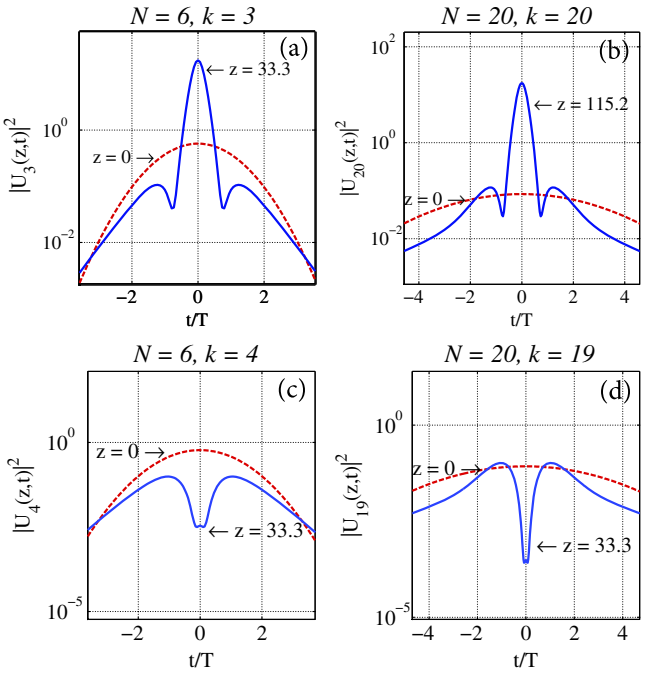

Fig. 4. Temporal profiles after the propagation of the input Gaussian pulses [Eq. (10)] (dashed line) with the initial parameters of $P = 0.61$ and $\tau = 1.5$. The pulse at the compression point (solid line) in shown for the third core (a), the fourth core (c), and for the 6-core MCF. Graphs (b) and (d) show similar temporal profiles for the pulses in 20th core (b) and 19th core (d), with the initial parameters of $P = 0.08035$ and $\tau = 3.85$ for the 20-core MCF.

Thus, we have demonstrated that one can effectively combine the pulse energy in MCFs. This type of nonlinear combining is essentially different from the currently popular schemes that rely on linear beam combining [17]. When using linear beam combining, it is critically important to control the phases of the separate beams. In our nonlinear combining scheme, the nonlinear interaction self-organizes the process of combining, and the phase and pulse shape perturbations at the MCF input are not very important. To demonstrate this feature, we consider the evolution of the pulses with random phase variations:

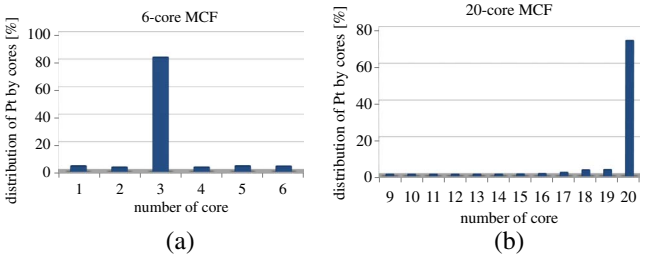

Fig. 5. Density distribution of the total energy E_t over the cores at the distance of $z = 33.3$ (a) The same at a distance of $z = 115.2$. (b) The maximum compression points corresponding to the propagation along the 6-core MCF. (a) The propagation along the 20-core fiber. (b) The propagation of the Gaussian pulses [Eq. (10)].

$$\tilde{U}_k = U_k \exp[-iC_\delta], \qquad k = 1\ldots N, \tag{11}$$

where $C_\delta = \delta f(k)$, with $f(k)$ being the pseudo-random function with values varying between −1 and 1. More specifically, we model $f(k)$ as $f(k) = \cos(5000k)$. The parameter δ varies from 0 to π, and consequently, C_δ takes values from $-\pi$ to π.

During the compression stage, the nonlinear interaction locked in the phases in the different cores and the initial phases affects only the threshold of the compression. The modeling demonstrates that the compression results are not very sensitive to the phase variations. Up to $\delta = 0.8$, the qualitative picture of the compression does not change and the compressed pulse is smooth. The percentage of power combined into one core does not change much, and the compression ratio is almost constant. For example, for $\delta = 0.7$ and $N = 20$, the pulse duration compression is about 16.8× and the peak power increases 202.5 times. About 75.6% of all initial power is concentrated into the first core. Notice that random initial phases can lead to a switch of the core where all of the power is concentrated. The length of compression is more sensitive to the phase fluctuations. For instance, for $\delta = 0$ and $N = 20$, the distance is $z_0 = 115.2$, while for $\delta = 0.7$, it is 56.1. In practice, a MCF has some fixed-length and phase variations that can affect the combining-compression performance. This problem can be fixed to a great extent with a deeper initial modulation of the intensity distribution in the cores, therefore making the system more resilient to phase fluctuations. Increasing the modulation parameter from 0.03 to 0.3 in Equation (10) significantly reduces the spread of the compression distances at different deltas. For example, for a 20-core MCF, $z_0 = 28.6$ when $\delta = 0$, and it reaches a minimum value of $z_0 = 26.1$ at $\delta = 0.5$.

Although our results are general and can be scaled to various system designs, let us make some numerical estimates for typical existing MCFs. Consider that $\beta_2 = -20$ ps^2/km and $\gamma = 1.5$ W^{-1} km^{-1}. The coupling coefficient parameter varies depending on the particular fiber. For telecom applications, the coupling must be low. For typical fibers, $C = 15.7$ km^{-1}, as seen in [14]. Coming back to the dimensional variable, we see that the unit of pulse duration T, $T^2 = -\beta_2/(2C)$, is about 0.8 ps and typically, the length $L = 1/C$ and 64 m. It means that our compressor must have a length of a few hundred meters and can compress the pulse up to about 100 fs. For our nonlinear compressor, one can build a MCF with more and closer-spaced cores, resulting in a MCF that has a larger coupling coefficient C. If C is increased up to $C \sim 1/m$, the length of the compressor is reduced to the few meters, and T is reduced to 0.1 psecs, compressions at pulse durations of ∼10 fs may be possible, although the model should be modified in this case.

Qualitatively, we anticipate that the ring configuration may be not the optimal scheme for maximum compression. The considered ring design (effectively 1D in k) is the equivalent of the 2D system in the continuous limit. Using 2D core distribution designs, we will have, in a corresponding continuous limit, an effective 3D NLSE with strongly collapsing features. It may be more practical to implement the pulse combining and compression in such configurations.

In conclusion, we have examined the pulse combining and compression in a ring MCF configuration. We have demonstrated the effective spatial focusing of energy to only a few cores through the pre-designed instability of the initial spatio-temporal light distribution. Further optimization of the proposed technique in various MCFs can lead to more efficient pulse compression and pulse combining.

This work was supported by the Russian Science Foundation (Grant No. 14-21-00110) and by the European Office of Aerospace Research and Development (Grant No. FA9550-14-1-0305) (work of S.K.T.). The work was partially performed under the auspices of the U.S. Department of Energy by the Lawrence Livermore National Laboratory under Contract DE-AC52-07NA27344.

References

1. D. J. Richardson, J. M. Fini, and L. E. Nelson, Nat. Photonics **7**, 354 (2013).
2. K. Igarashi, T. Tsuritani, and I. Morita,"1-exabit/s×km super-Nyquist-WDM multi-core-fiber transmission," *ECOC*, Cannes (2014).
3. A. B. Aceves, G. G. Luther, C. De Angelis, A. M. Rubenchik, and S. K. Turitsyn, Phys. Rev. Lett. **75**, 73 (1995).
4. A. B. Aceves, G. G. Luther, C. De Angelis, A. M. Rubenchik, and S. K. Turitsyn, Opt. Fiber Technol. **1**, 244 (1995).
5. C. Agger, S. T. Srensen, C. L. Thomsen, S. R. Keiding, and O. Bang, Opt. Lett. **36**, 2596 (2011).
6. S. K. Turitsyn, A. M. Rubenchik, M. P. Fedoruk, and E. Tkachenko, Phys. Rev. A **86**, 031804 (2012).
7. A. M. Rubenchik, E. V. Tkachenko, M. P. Fedoruk, and S. K. Turitsyn, Opt. Lett. **38**, 4232 (2013).
8. S. K. Turitsyn, Phys. Rev. A **47**, R27 (1993).
9. Y. Silberberg, Opt. Lett. **15**, 1282 (1990).
10. S. Minardi, F. Eilenberger, Y. V. Kartashov, A. Szameit, U. Röpke, J. Kobelke, K. Schuster, H. Bartelt, S. Nolte, L. Torner, F. Lederer, A. Tünnermann, and T. Pertsch, Phys. Rev. Lett. **105**, 263901 (2010).
11. T. X. Tran, D. C. Duong, and F. Biancalana, Phys. Rev. A **90**, 023857 (2014).
12. Y. S. Kivshar and G. P. Agrawal, *Optical Solitons: From Fibers to Photonic Crystals*, 5th ed. (Academic, 2003).
13. A. B. Aceves, A. M. Rubenchik, S. K. Turitsyn, and C. De Angelis, Opt. Lett. **19**, 329 (1994).
14. S. Mumtaz, R. Essiambre, and G. Agrawal, IEEE Photon. Technol. Lett. **24**, 1574 (2012).
15. S. K. Turitsyn, B. G. Bale, and M. P. Fedoruk, Phys. Rep. **521**, 135 (2012).
16. N. Higham, SIAM J. Matrix Anal. Appl. **26**, 1179 (2005).
17. T. Fan, IEEE J. Sel. Top. Quantum Electron. **11**, 567 (2005).